Thermodynamic theory of the shock wave structure in a rarefied polyatomic gas: Beyond the Bethe-Teller theory

Shigeru Taniguchi,[1,*] Takashi Arima,[2,†] Tommaso Ruggeri,[3,‡] and Masaru Sugiyama[1,§]
[1]*Graduate School of Engineering, Nagoya Institute of Technology, Nagoya 466-8555, Japan*
[2]*Center for Social Contribution and Collaboration, Nagoya Institute of Technology, Nagoya 466-8555, Japan*
[3]*Department of Mathematics, University of Bologna, Bologna, Italy*
(Received 8 October 2013; published 31 January 2014)

The structure of a shock wave in a rarefied polyatomic gas is studied on the basis of the theory of extended thermodynamics. Three types of the shock wave structure observed in experiments, that is, the nearly symmetric shock wave structure (type A, small Mach number), the asymmetric structure (type B, moderate Mach number), and the structure composed of thin and thick layers (type C, large Mach number), are explained by the theory in a unified way. The theoretical prediction of the profile of the mass density agrees well with the experimental data. The well-known Bethe-Teller theory of the shock wave structure in a polyatomic gas is reexamined in the light of the present theory.

DOI: 10.1103/PhysRevE.89.013025 PACS number(s): 47.45.−n, 05.70.Ln

I. INTRODUCTION

Characteristic features of the shock wave structure in a rarefied *polyatomic* gas are quite different from those in a rarefied monatomic gas due to the presence of the microscopic internal modes in a polyatomic molecule, namely, the rotational and vibrational modes [1,2]. We here mention two typical features: (1) It is well known that the shock wave thickness in a rarefied monatomic gas is of the order of the mean free path. On the other hand, owing to the slow relaxation process of the internal modes, the thickness of a shock wave in a rarefied polyatomic gas is several orders larger than the mean free path. It can be several centimeters long. (2) As the Mach number increases from unity, the profile of the shock wave structure in a polyatomic rarefied gas changes from the nearly symmetric profile (type A) to the asymmetric profile (type B), and then changes further to the profile composed of thin and thick layers (type C) [3–8]. Schematic profiles of the mass density are shown in Fig. 1. These peculiar changes of the shock wave profile with the Mach number cannot be observed in a monatomic gas.

In order to explain the shock wave structure in a rarefied polyatomic gas, two different approaches (I) and (II) were proposed more than a half century ago:

(I) An approach was proposed by Bethe and Teller [9]. In their celebrated theory, at the very beginning, the internal degrees of freedom of a molecule are assumed to be classified into two parts: the one part is composed of the "active" degrees of freedom that relax instantaneously, and the other part is composed of the "inert" degrees of freedom that relax slowly with a finite relaxation time. Except for hydrogen gas, the translational and rotational modes are regarded as the active degrees of freedom but the vibrational modes are considered as inert degrees of freedom. In order to analyze the thin layer Δ shown in Fig. 1, the system of Euler equations is adopted. The Rankine-Hugoniot conditions of the system for jumps of the physical quantities at Δ are derived under the following assumption: The internal energy due to the inert degrees of freedom is unchanged in the thin layer Δ because only active degrees of freedom are able to adjust to such an instantaneous change. Therefore, exactly speaking, the thin layer in this theory is just the jump discontinuity with no thickness. In order to analyze the relaxation process in the thick layer Ψ in Fig. 1, a variant of the Euler system with an additional linear relaxation equation for the internal vibrational modes is adopted.

This approach can describe the shock wave structure of type C. The jumps of the physical quantities at the thin layer Δ can be calculated without using any adjustable parameters. The agreement between the theoretical predictions and the existing experimental data seems to be good.

It should be emphasized, however, that the basis of the Bethe-Teller theory is not clear enough. The assumption of the classification of the internal degrees of freedom should be regarded as a rough approximation even though it seems to be plausible intuitively. As the classification is not so clear-cut in reality, it may introduce some arbitrariness into the theory. And furthermore two different systems of equations are adopted in this theory for analyzing the thin and thick layers separately. The compatibility between the two systems is, however, unclear from both mathematical and physical points of view. It is highly preferable, of course, to have one unified system of equations from which all types A, B, and C can be derived in a fully consistent way.

(II) The other approach, which originates from the work by Gilbarg and Paolucci [10], is basing on the system of the Navier-Stokes Fourier (NSF) equations. They studied, as a typical example, the shock wave structure in rarefied carbon dioxide (CO_2) gas by adopting a very large value of the bulk viscosity. Although they could predict a thick shock wave structure, the shock profiles are always symmetric (type A). No asymmetric shock wave structure (type B) nor thin layer (type C) could be explained by this theory.

One crucial point to be noted is that, because the NSF theory is constructed with the assumption of local equilibrium [11], the theory is, in general, unsatisfactory for analyzing highly

*taniguchi@stat.nitech.ac.jp
†tks@stat.nitech.ac.jp
‡tommaso.ruggeri@unibo.it
§sugiyama@nitech.ac.jp

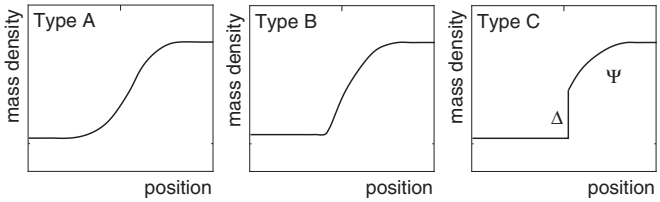

FIG. 1. Three types of shock wave structure in a rarefied polyatomic gas. As the Mach number increases from unity, the profile of the shock wave structure changes from type A to type B, and then to type C. The profile of type C consists of the thin layer Δ and the thick layer Ψ.

nonequilibrium phenomena such as shock wave phenomena. Fortunately we have alternative theories as discussed below.

For rarefied monatomic gases, there already exist theories which can describe phenomena out of local equilibrium, that is, kinetic theory with the use of the Boltzmann equation (the Chapman-Enskog method [12] and the moment method [13]), and the theories of extended thermodynamics (ET) [14] and of molecular extended thermodynamics with closure by the maximum entropy principle [15,16]. These theories can indeed describe the structure of strong shock waves in a rarefied monatomic gas [14,17]. Numerical techniques for solving the Boltzmann equation, such as the direct simulation Monte Carlo method [18], have also been developed, and their usefulness has been confirmed through comparison between their predictions and the experimental data.

For rarefied polyatomic gases, kinetic theory (the Chapman-Enskog method [12] and the moment method [19–22]) has been developed. Numerical methods for solving the Boltzmann equation have also been developed [18]. However, as the appropriate modeling of the collision term in the Boltzmann equation between two polyatomic molecules is very complicated, some simplifications are usually introduced into the modeling. It is therefore not self-evident that the numerical results thus obtained are compatible with the second law of thermodynamics. There is, however, still another theory, that is, the ET theory of polyatomic gases, which was proposed recently by the present authors [23,24]. It is notable that, as summarized briefly in the next section, the ET theory is totally free from the difficult problems mentioned just above. The corresponding molecular ET theory was also presented [25].

The purpose of the present paper is to use the ET theory to study shock wave structures of types A–C in a rarefied polyatomic gas. We will show how to overcome the difficulties encountered in the previous approaches (I) and (II).

The organization of the paper is as follows: In Sec. II, the essential idea of the ET theory of rarefied polyatomic gases and dense gases is summarized. In Sec. III, the basic equations for our analysis derived from the ET theory are summarized. In Sec. IV, the conditions for the present analysis are summarized. The parameters in the system and the numerical method are also explained. In Sec. V, the main results of the shock wave structure in the present analysis are shown and discussed. The predictions derived from the ET theory are also compared with those from NSF theory. The Bethe-Teller theory is reexamined in the light of the present theory. In Sec. VI, a comparison between the theoretical predictions derived from the ET theory and the experimental data is made. Section VII is devoted to the summary and outlook. In the Appendix, the NSF theory for studying the shock wave structure is briefly summarized.

II. EXTENDED THERMODYNAMICS OF REAL GASES

The ET theory of rarefied polyatomic gases and of dense gases [23,24] is briefly summarized.

A. Binary hierarchy of the differential equations

In the ET theory, the dissipative fluxes are also adopted as independent variables in addition to the usual independent variables used in the NSF theory. We adopt, as the simplest and natural extension of the NSF theory, the ET theory with the following 14 independent variables (ET14) [23,24]; the mass density ρ, the velocity v_i, the temperature T, the dynamic pressure (nonequilibrium pressure) Π, the shear stress $\sigma_{\langle ij\rangle}$, and the heat flux q_i, where $i,j = 1,2,3$, and the angular brackets in $\sigma_{\langle ij\rangle}$ indicate that the shear stress is a deviatoric (that is, symmetric traceless) tensor.

We assume the following binary hierarchy (F series and G series) of the balance equations:

$$\begin{aligned} &\frac{\partial F}{\partial t} + \frac{\partial F_k}{\partial x_k} = 0, \\ &\frac{\partial F_i}{\partial t} + \frac{\partial F_{ik}}{\partial x_k} = 0, \quad \frac{\partial G_{ii}}{\partial t} + \frac{\partial G_{iik}}{\partial x_k} = 0, \\ &\frac{\partial F_{ij}}{\partial t} + \frac{\partial F_{ijk}}{\partial x_k} = P_{ij}, \quad \frac{\partial G_{ppi}}{\partial t} + \frac{\partial G_{ppik}}{\partial x_k} = Q_{ppi}, \end{aligned} \tag{1}$$

where F is the mass density, F_i is the momentum density, and F_{ij} is the momentum flux. G_{ii} and G_{ppi} are proportional to the energy density and the energy flux, respectively. Here F_{ijk} and G_{ppik} are the fluxes of F_{ij} and G_{ppi}, and P_{ij} and Q_{ppi} are the productions. Summation on repeated indices is assumed throughout the present paper. The equations with no production term represent the mass, momentum, and energy conservation laws and therefore we have the following relations:

$$\begin{aligned} &F = \rho, \quad F_i = \rho v_i, \quad G_{ii} = 2\rho\varepsilon + \rho v_i v_i, \\ &F_{ij} = \rho v_i v_j + (p + \Pi)\delta_{ij} - \sigma_{\langle ij\rangle}, \\ &G_{ppi} = \rho v_p v_p v_i + 2\rho\varepsilon v_i + 2v_p\{(p + \Pi)\delta_{pi} - \sigma_{\langle pi\rangle}\} + 2q_i, \end{aligned}$$

where ε and p are the specific internal energy and the pressure.

As the balance equations (1) should be invariant under a *Galilean transformation*, the dependence of the quantities on the velocity can be determined [26]:

$$\begin{aligned} F_{ijk} &= \rho v_i v_j v_k + (p + \Pi)(v_i\delta_{jk} + v_j\delta_{ki} + v_k\delta_{ij}) \\ &\quad - v_i\sigma_{\langle jk\rangle} - v_j\sigma_{\langle ki\rangle} - v_k\sigma_{\langle ij\rangle} + M_{ijk}, \\ G_{ppik} &= \rho v_p v_p v_i v_k + 2\rho\varepsilon v_i v_k + (p + \Pi)(v_p v_p\delta_{ik} + 4v_i v_k) \\ &\quad - \sigma_{\langle ik\rangle} v_p v_p - 2\sigma_{\langle pi\rangle} v_p v_k - 2\sigma_{\langle pk\rangle} v_p v_i \\ &\quad + 2q_i v_k + 2q_k v_i + 2v_p M_{pik} + m_{ppik}, \\ Q_{ppi} &= Q_i + 2v_p P_{pi}, \end{aligned}$$

where M_{ijk}, m_{ppik}, Q_i, and P_{pi} are velocity-independent quantities.

B. Constitutive theory

We need the constitutive equations for M_{ijk}, m_{ppik}, Q_i, and P_{pi} in order to obtain a closed system of field equations. We assume that the constitutive equations at one point and time depend on the independent fields at that point and time. We apply the constitutive theory of ET [14] where the following universal physical principles (A)–(C) are imposed on the constitutive equations:

(A) *Material frame indifference principle*. This requires that the constitutive equations are independent of an observer. This principle and the Galilean invariance for the balance laws constitute the objectivity principle.

(B) *Entropy principle*. All solutions of the system of field equations must satisfy the entropy balance law:

$$\frac{\partial h}{\partial t}+\frac{\partial h_k}{\partial x_k}=\Sigma\geqq 0,$$

where h is the entropy density, h_k is the entropy flux, and Σ is the entropy production. Here h and h_k are constitutive quantities.

(C) *Causality*. This requires concavity of the entropy density and guarantees the hyperbolicity of the system of field equations. This also ensures the well-posedness (local in time) of a Cauchy problem and the finiteness of the propagation speeds of disturbances.

C. Field equations

We can derive the closed system of field equations by using the constitutive equations and the caloric and thermal equations of state $p=p(\rho,T)$ and $\varepsilon=\varepsilon(\rho,T)$. Because the system of field equations is quite lengthy, we here omit its explicit expression. For all the details, please consult Refs. [23,24].

D. Some remarks

The theory with kinetic equations for polyatomic gases [19,20] has 17 independent fields, while the present phenomenological continuum theory uses only 14 independent fields, which also appear in the NSF theory. Because of this the NSF theory can be derived naturally, as a limiting case, from the present theory. These 14 fields have well-established physical meanings.

The ET14 theory was proved to be fully consistent with the kinetic approach for polyatomic rarefied gases [27,28]. In fact, as pointed out above, Pavić, Ruggeri, and Simić have proven [25], using the closure of the maximum entropy principle [16], the perfect coincidence with the system obtained by the macroscopic ET approach [23].

The usefulness of the ET theory was confirmed by the fact that the dispersion relation for ultrasonic sound in rarefied diatomic gases agrees well with the experimental data even in the high-frequency range where the NSF theory is no longer valid [29]. It has also been proved [30] that the theory can be regarded as a generalization of the Meixner theory of relaxation processes [31,32]. An ET theory for moderately dense gases has also been proposed in the papers cited above [23,24].

III. BASIC EQUATIONS

In this section, we summarize the basic equations for the present analysis.

A. Equations of state

We adopt the following caloric and thermal equations of state for a rarefied polyatomic gas:

$$\varepsilon=\varepsilon(T),\quad p=\rho\frac{k_B}{m}T, \tag{2}$$

where k_B and m are, respectively, the Boltzmann constant and the mass of a molecule. The functional form of the specific internal energy ε is determined through the specific heat c_v:

$$\varepsilon(T)=\frac{k_B}{m}\int_{T_R}^{T}\hat{c}_v(\xi)\,d\xi, \tag{3}$$

where $\hat{c}_v\equiv(m/k_B)c_v$ is the dimensionless specific heat and T_R is an inessential reference temperature. We may determine the temperature dependence of $\hat{c}_v$ from the experimental data and/or statistical-mechanical considerations. By using the relations (2) and (3), we have the sound velocity expressed as [29]

$$c=\sqrt{\frac{k_B}{m}T\gamma(T)}, \tag{4}$$

where $\gamma(T)=[1+\hat{c}_v(T)]/\hat{c}_v(T)$ is the ratio of the specific heats.

B. Balance equations derived from the theory of extended thermodynamics

As we analyze one-dimensional (plane) shock waves propagating along the x axis, the vectorial and tensorial quantities are expressed by

$$v_i\equiv\begin{pmatrix}v\\0\\0\end{pmatrix},\quad \sigma_{\langle ij\rangle}\equiv\begin{pmatrix}\sigma&0&0\\0&-\frac{1}{2}\sigma&0\\0&0&-\frac{1}{2}\sigma\end{pmatrix},$$
$$q_i\equiv\begin{pmatrix}q\\0\\0\end{pmatrix}. \tag{5}$$

The system of equations for the 14 fields in the present problem is given by [23]

$$\frac{\partial\rho}{\partial t}+\frac{\partial}{\partial x}(\rho v)=0,\quad \frac{\partial\rho v}{\partial t}+\frac{\partial}{\partial x}(p+\Pi-\sigma+\rho v^2)=0,\quad \frac{\partial}{\partial t}(2\rho\varepsilon+\rho v^2)+\frac{\partial}{\partial x}\{2\rho\varepsilon v+2(p+\Pi-\sigma)v+\rho v^3+2q\}=0,$$
$$\frac{\partial}{\partial t}\{3(p+\Pi)+\rho v^2\}+\frac{\partial}{\partial x}\left\{(5p+5\Pi-2\sigma)v+\rho v^3+\frac{5}{1+\hat{c}_v}q\right\}=-\frac{3\Pi}{\tau_\Pi},$$

$$\frac{\partial}{\partial t}(p+\Pi-\sigma+\rho v^2)+\frac{\partial}{\partial x}\left\{3(p+\Pi-\sigma)v+\rho v^3+\frac{3}{1+\hat{c}_v}q\right\}=\frac{\sigma}{\tau_S}-\frac{\Pi}{\tau_\Pi},$$
$$\frac{\partial}{\partial t}\{2\rho\varepsilon v+2(p+\Pi-\sigma)v+\rho v^3+2q\}+\frac{\partial}{\partial x}\left\{2\rho\varepsilon v^2+5(p+\Pi-\sigma)v^2+\rho v^4+2\left(\varepsilon+\frac{k_B}{m}T\right)p\right.$$
$$\left.+2\left(\varepsilon+2\frac{k_B}{m}T\right)(\Pi-\sigma)+\frac{10+4\hat{c}_v}{1+\hat{c}_v}qv\right\}=-2\left\{\frac{q}{\tau_q}+\left(\frac{\Pi}{\tau_\Pi}-\frac{\sigma}{\tau_S}\right)v\right\}, \tag{6}$$

where τ_Π, τ_S, and τ_q are the relaxation times for the dynamic pressure, the shear stress, and the heat flux, respectively. The relaxation times are related to the phenomenological coefficients as follows [23]:

$$\mu=p\tau_S,\quad \nu=\left(\frac{2}{3}-\frac{1}{\hat{c}_v}\right)p\tau_\Pi,\quad \kappa=(1+\hat{c}_v)\frac{k_B}{m}p\tau_q, \tag{7}$$

where μ, ν, and κ are, respectively, the shear viscosity, the bulk viscosity, and the heat conductivity. In general the relaxation times are functions of the mass density ρ and the temperature T.

The characteristic velocities λ of the hyperbolic system (6) evaluated in equilibrium are

$$\frac{\lambda}{c}=0,0,\pm\sqrt{\frac{\hat{c}_v\left(7+4\hat{c}_v-\sqrt{37+32\hat{c}_v+4\hat{c}_v^2}\right)}{2(1+\hat{c}_v)^2}},\pm\sqrt{\frac{\hat{c}_v\left(7+4\hat{c}_v+\sqrt{37+32\hat{c}_v+4\hat{c}_v^2}\right)}{2(1+\hat{c}_v)^2}}. \tag{8}$$

The characteristic velocities play an essential role in studies of nonlinear wave propagation, in particular, shock wave propagation. The ET theory gives a differential system of hyperbolic type and, as a consequence, it predicts a shock wave structure with a discontinuous part when the Mach number becomes large. According to the theorem of Boillat and Ruggeri [33], a subshock, which is obtained as a weak solution of the system of equations, emerges when the shock velocity s exceeds the maximum characteristic velocity $\lambda_{\max}$ of the hyperbolic system. The value of $\lambda_{\max}$ in the case of rarefied CO_2 gas will be given below.

IV. SETTING OF THE PROBLEM

In this section the conditions that we adopt for the present analysis are summarized. The parameters are fixed and the numerical method for the computation is explained.

As the differential system is Galilean invariant, we can consider, without loss of generality, that the shock wave is stationary, using a coordinate system moving with the shock wave, that is, a comoving coordinate system. Both the *unperturbed state* (the state at $x=-\infty$ before and far from a shock wave) and the *perturbed state* (the state at $x=\infty$ after and far from a shock wave) are assumed to be in thermal equilibrium.

A. Dimensionless form of the field equations

For convenience we introduce the following dimensionless quantities:

$$\hat{\rho}\equiv\frac{\rho}{\rho_0},\quad \hat{v}\equiv\frac{v}{c_0},\quad \hat{T}\equiv\frac{T}{T_0},\quad \hat{\sigma}\equiv\frac{\sigma}{\rho_0\frac{k_B}{m}T_0},\quad \hat{\Pi}\equiv\frac{\Pi}{\rho_0\frac{k_B}{m}T_0},\quad \hat{q}\equiv\frac{q}{\rho_0\frac{k_B}{m}T_0c_0},$$
$$\hat{x}\equiv\frac{x}{\tau_\Pi(\rho_0,T_0)c_0},\quad \hat{t}\equiv\frac{t}{\tau_\Pi(\rho_0,T_0)},\quad \hat{\tau}_\Pi\equiv\frac{\tau_\Pi(\rho,T)}{\tau_\Pi(\rho_0,T_0)},\quad \hat{\tau}_S\equiv\frac{\tau_S(\rho,T)}{\tau_\Pi(\rho_0,T_0)},\quad \hat{\tau}_q\equiv\frac{\tau_q(\rho,T)}{\tau_\Pi(\rho_0,T_0)}, \tag{9}$$

where the quantities with subscript 0 represent the quantities in the unperturbed state. The balance equations (6) are now rewritten in terms of the dimensionless quantities as follows:

$$\frac{d}{d\hat{x}}(\hat{\rho}\hat{v})=0,$$
$$\frac{d}{d\hat{x}}\left\{\frac{1}{\gamma_0}(\hat{\rho}\hat{T}+\hat{\Pi}-\hat{\sigma})+\hat{\rho}\hat{v}^2\right\}=0,$$
$$\frac{d}{d\hat{x}}\left\{\frac{2}{\gamma_0}\left(\hat{\rho}\hat{v}\frac{1}{T_0}\int_{T_R}^{T}\hat{c}_v(\xi)\,d\xi+(\hat{\rho}\hat{T}+\hat{\Pi}-\hat{\sigma})\hat{v}+\hat{q}\right)+\hat{\rho}\hat{v}^3\right\}=0,$$
$$\frac{d}{d\hat{x}}\left\{\frac{1}{\gamma_0}\left((5\hat{\rho}\hat{T}+5\hat{\Pi}-2\hat{\sigma})\hat{v}+\frac{5}{\hat{c}_v(T)+1}\hat{q}\right)+\hat{\rho}\hat{v}^3\right\}=-\frac{3}{\gamma_0}\frac{\hat{\Pi}}{\hat{\tau}_\Pi},$$
$$\frac{d}{d\hat{x}}\left\{\frac{3}{\gamma_0}\left((\hat{\rho}\hat{T}+\hat{\Pi}-\hat{\sigma})\hat{v}+\frac{1}{\hat{c}_v(T)+1}\hat{q}\right)+\hat{\rho}\hat{v}^3\right\}=\frac{1}{\gamma_0}\left(\frac{\hat{\sigma}}{\hat{\tau}_S}-\frac{\hat{\Pi}}{\hat{\tau}_\Pi}\right),$$

$$\frac{d}{d\hat{x}}\left[\frac{1}{\gamma_0}\left\{\left(\frac{1}{\gamma_0}(\hat{\rho}\hat{T}+\hat{\Pi}-\sigma)+\hat{\rho}\hat{v}^2\right)\frac{2}{T_0}\int_{T_R}^{T}\hat{c}_v(\xi)\,d\xi+\frac{2}{\gamma_0}\hat{T}(\hat{\rho}\hat{T}+2\hat{\Pi}-2\hat{\sigma})+5(\hat{\rho}\hat{T}+\hat{\Pi}-\hat{\sigma})\hat{v}^2\right.\right.$$
$$\left.\left.+\frac{4\hat{c}_v(T)+10}{\hat{c}_v(T)+1}\hat{q}\hat{v}\right\}+\hat{\rho}\hat{v}^4\right]=-\frac{2}{\gamma_0}\left\{\frac{\hat{q}}{\hat{\tau}_q}+\left(\frac{\hat{\Pi}}{\hat{\tau}_\Pi}-\frac{\hat{\sigma}}{\hat{\tau}_S}\right)\hat{v}\right\}, \tag{10}$$

where $\gamma_0 \equiv \gamma(T_0)$. As the conservation laws $(10)_{1\text{–}3}$ can be easily integrated, we can simplify the balance equations as follows:

$$\hat{\rho}=\frac{M_0}{\hat{v}},\quad \frac{1}{\gamma_0}\left(\frac{M_0\hat{T}}{\hat{v}}+\hat{\Pi}-\hat{\sigma}\right)+M_0\hat{v}=\frac{1}{\gamma_0}+M_0^2,$$
$$\frac{2}{\gamma_0}\left(\frac{M_0}{T_0}\int_{T_0}^{T}\hat{c}_v(\xi)\,d\xi+M_0\hat{T}+\hat{\Pi}\hat{v}-\hat{\sigma}\,\hat{v}+\hat{q}\right)+M_0\hat{v}^2=\frac{2}{\gamma_0}M_0+M_0^3,$$
$$\frac{d}{d\hat{x}}\left\{\frac{1}{\gamma_0}\left(5M_0\hat{T}+5\hat{\Pi}\hat{v}-2\hat{\sigma}\,\hat{v}+\frac{5}{\hat{c}_v(T)+1}\hat{q}\right)+M_0\hat{v}^2\right\}=-\frac{3}{\gamma_0}\frac{\hat{\Pi}}{\hat{\tau}_\Pi},$$
$$\frac{d}{d\hat{x}}\left\{\frac{3}{\gamma_0}\left((M_0\hat{T}+\hat{\Pi}\hat{v}-\hat{\sigma}\,\hat{v})+\frac{1}{\hat{c}_v(T)+1}\hat{q}\right)+M_0\hat{v}^2\right\}=\frac{1}{\gamma_0}\left(\frac{\hat{\sigma}}{\hat{\tau}_S}-\frac{\hat{\Pi}}{\hat{\tau}_\Pi}\right),$$
$$\frac{d}{d\hat{x}}\left[\frac{1}{\gamma_0}\left\{\left(\frac{1}{\gamma_0}+M_0^2\right)\frac{2}{T_0}\int_{T_R}^{T}\hat{c}_v(\xi)\,d\xi+\frac{2}{\gamma_0}\hat{T}\left(\frac{M_0\hat{T}}{\hat{v}}+2\hat{\Pi}-2\hat{\sigma}\right)+5(M_0\hat{T}+\hat{\Pi}\hat{v}-\hat{\sigma}\,\hat{v})\hat{v}+\frac{4\hat{c}_v(T)+10}{\hat{c}_v(T)+1}\hat{q}\hat{v}\right\}+M_0\hat{v}^3\right]$$
$$=-\frac{2}{\gamma_0}\left\{\frac{\hat{q}}{\hat{\tau}_q}+\left(\frac{\hat{\Pi}}{\hat{\tau}_\Pi}-\frac{\hat{\sigma}}{\hat{\tau}_S}\right)\hat{v}\right\}, \tag{11}$$

where M_0 represents the Mach number in the unperturbed state, expressed by

$$M_0 \equiv \frac{v_0}{c_0}. \tag{12}$$

B. Boundary conditions: Rankine-Hugoniot conditions for the system of Euler equations

The boundary conditions for the basic system of equations expressed above are determined as follows: By inserting $\hat{\Pi}=0$, $\hat{\sigma}=0$, and $\hat{q}=0$ into $(11)_{1\text{–}3}$, we obtain the expressions for the quantities in the perturbed state:

$$\hat{\rho}_1=\frac{M_0}{\hat{v}_1},\quad \frac{1}{\gamma_0}\left(\frac{M_0\hat{T}_1}{\hat{v}_1}-1\right)+M_0\,(\hat{v}_1-M_0)=0,$$
$$\frac{2}{\gamma_0}M_0\left(\hat{T}_1+\frac{1}{T_0}\int_{T_0}^{T_1}\hat{c}_v(\xi)\,d\xi-1\right)+M_0\left(\hat{v}_1^2-M_0^2\right)=0, \tag{13}$$

where the quantities with subscript 1 are those in the perturbed state. These relations express the Rankine-Hugoniot conditions for the system of Euler equations.

C. Parameters

In order to compare the theoretical predictions with experimental data, we will focus our study on the experimental data for the shock wave structure in rarefied CO_2 gas at $T=295$ K and $p=69$ mm Hg in the unperturbed state [7]. We have determined the dependence of the specific heat on the temperature, which is shown in Fig. 2, by inserting the data on the temperature dependence of the sound velocity [34] into (4). The values of the dimensionless specific heat $\hat{c}_v$, sound velocity c_0, heat conductivity κ [35], and shear viscosity μ [35] in the unperturbed state are summarized in Table I. We note that the rotational modes are completely excited and the vibrational modes are partially excited at this temperature. From (8), the maximum characteristic velocity at $T=295$ K is estimated as $\lambda_{\max}/c \approx 1.74$. Therefore we recognize that the shock wave structure predicted by the theory is continuous up to $M_0 \approx 1.74$.

For a rarefied CO_2 gas, the temperature dependence of the phenomenological coefficients was already estimated by both kinetic theoretical considerations and the experimental

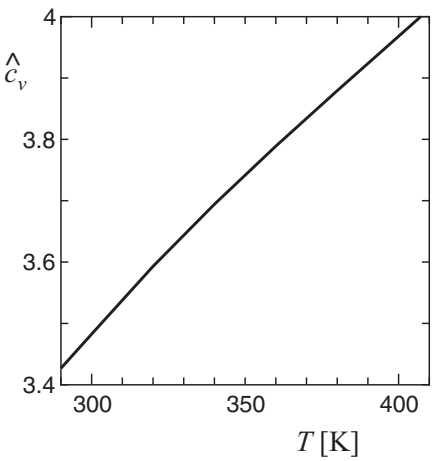

FIG. 2. Dependence of the dimensionless specific heat of a rarefied CO_2 gas on the temperature [34].

TABLE I. Experimental values of the dimensionless specific heat $\hat{c}_v$ [34], sound velocity c_0 [34], heat conductivity κ [35], and shear viscosity μ [35] of a rarefied CO_2 gas at $T = 295$ K and $p = 69$ mm Hg.

	$\hat{c}_v$	c_0 (m/s)	κ (W/m K)	μ (Pa s)
CO_2	3.45	269	1.68×10^{-2}	1.5×10^{-5}

data [10] as follows:

$$\mu \propto T^n, \quad \nu \propto T^n, \quad \kappa \propto T^n \hat{c}_v(T), \tag{14}$$

where the exponent n was estimated as $n = 0.935$. We adopt the same temperature dependence in the present analysis. We have confirmed that the shock wave structure studied below depends weakly on the value of the exponent n.

By substituting (14) into the relation (7), we have the following dependence of the relaxation times on the mass density and the temperature:

$$\begin{aligned} \hat{\tau}_\Pi &= \frac{1}{\hat{\rho}\hat{T}^{1-n}} \frac{5-3\gamma_0}{5-3\gamma(T)}, \\ \hat{\tau}_S &= \frac{\tau_S(\rho_0,T_0)}{\tau_\Pi(\rho_0,T_0)} \frac{1}{\hat{\rho}\hat{T}^{1-n}}, \\ \hat{\tau}_q &= \frac{\tau_q(\rho_0,T_0)}{\tau_\Pi(\rho_0,T_0)} \frac{1}{\hat{\rho}\hat{T}^{1-n}} \frac{\gamma_0}{\gamma(T)}. \end{aligned} \tag{15}$$

Inserting the values of the phenomenological coefficients in Table I into the relations (7), we obtain the values of the relaxation times τ_S and τ_q for the shear stress and the heat flux in the unperturbed state as shown in Table II. The only remaining undetermined parameter is the relaxation time τ_Π for the dynamic pressure, which is proportional to the bulk viscosity ν. Because of the lack of knowledge of reliable data on ν due to the difficulty in its experimental measurements, we will use τ_Π in the unperturbed state as a fitting parameter. As will be explained below, the value of τ_Π in the unperturbed state is determined by the comparison of the theoretical prediction with the experimental data for $M_0 = 1.47$. See also Figs. 6 and 7 below. It is noticeable that the value of τ_Π is larger, with a different order of magnitude, than the other two relaxation times.

D. Numerical methods

We solve numerically the system of balance equations (11) under the boundary conditions (13) by adopting the methods proposed by Weiss [14,36]. We introduce $N+1$ grid points such that the range $[-\hat{L}/2, \hat{L}/2]$ on the $\hat{x}$ axis is discretized with constant intervals $\Delta\hat{x} = \hat{L}/N$ as follows:

$$\hat{x}^i = -\frac{\hat{L}}{2} + \frac{\hat{L}}{N} i \quad \text{for } i = 0,1,\ldots,N, \tag{16}$$

where the superscript i represents the number of the grid point.

Because the mass density $\hat{\rho}$ is already expressed by other variables in $(11)_1$, we need to solve the system $(11)_{2-6}$ for $\mathbf{u} = (\hat{v}, \hat{T}, \hat{\Pi}, \hat{\sigma}, \hat{q})$. The boundary conditions (13) give

$$\mathbf{u}^0 = \mathbf{u}_0, \quad \mathbf{u}^N = \mathbf{u}_1, \tag{17}$$

where $\mathbf{u}^i$ represents $\mathbf{u}|_{\hat{x}=\hat{x}^i}$, $\mathbf{u}_0 = (M_0,1,0,0,0)$, and $\mathbf{u}_1 = (\hat{v}_1, \hat{T}_1, 0,0,0)$. For the conservation laws $(11)_{2,3}$ expressed as $\mathbf{F}(\mathbf{u}) = \mathbf{F}(\mathbf{u}_0)$ with $\mathbf{F}$ being the general flux, we have

$$\mathbf{F}(\mathbf{u}^i) = \mathbf{F}(\mathbf{u}_0) \quad \text{for } i = 1,2,\ldots,N-1. \tag{18}$$

Replacing the differentiation in the balance equations $(11)_{4-6}$, which we express as $d\mathbf{F}(\mathbf{u})/d\hat{x} = \mathbf{P}(\mathbf{u})$ compactly with $\mathbf{P}$ being the general production, by the central difference, we get

$$\frac{\mathbf{F}(\mathbf{u}^{i+1}) - \mathbf{F}(\mathbf{u}^{i-1})}{2\Delta\hat{x}} = \mathbf{P}(\mathbf{u}^i) \quad \text{for } i = 1,2,\ldots,N-1. \tag{19}$$

The nonlinear algebraic equations (18) and (19) with the condition (17) may be solved with the help of numerical solvers equipped with software for numerical computations. In the present analysis, we have constructed numerical codes by adopting the numerical solver implemented in MATHEMATICA based on Newton's method. The computation starts from an appropriate initial guess, e.g.,

$$\mathbf{u}^i = \begin{cases} \mathbf{u}_0 & \text{for } i = 0,1,\ldots,\frac{N}{2}, \\ \mathbf{u}_1 & \text{for } i = \frac{N}{2}+1, \frac{N}{2}+2, \ldots, N, \end{cases} \tag{20}$$

and iterative calculations are repeated until the numerical solution converges to the one that satisfies the system (11) and the boundary conditions (13) within the appropriate accuracy we have set; eight digits of precision in the present analysis. We have chosen $\Delta\hat{x}$ small enough and have confirmed that the dependence of the profiles in Figs. 3–7 on $\Delta\hat{x}$ is negligibly small.

TABLE II. Relaxation times for CO_2 gas at $T = 295$ K and $p = 69$ mm Hg. The relaxation times τ_S and τ_q are obtained from the experimental data shown in Table I. Only the relaxation time for the dynamic pressure τ_Π remains as a fitting parameter.

	$\tau_S(\rho_0,T_0)$ (s)	$\tau_q(\rho_0,T_0)$ (s)	$\tau_\Pi(\rho_0,T_0)$ (s)
CO_2	1.6×10^{-9}	2.2×10^{-9}	2.2×10^{-5}

V. SHOCK WAVE STRUCTURE

In this section, we show and emphasize that all of the three types of shock wave structure, types A to C, can be described naturally within the present theory. The details of types A to C are explained and discussed in this order.

A. Type A: Nearly symmetric shock wave structure

The nearly symmetric shock wave structure appears in a small Mach number region just above unity. A typical example of the shock wave structure of type A is obtained at $M_0 = 1.04$ as shown in Fig. 3. We have depicted the profiles of all independent variables; the mass density, the velocity, the temperature, the dynamic pressure, the shear stress, and the heat flux. We can confirm that the shock wave structure is indeed nearly the same as the one predicted by the NSF theory, which is summarized briefly in the Appendix.

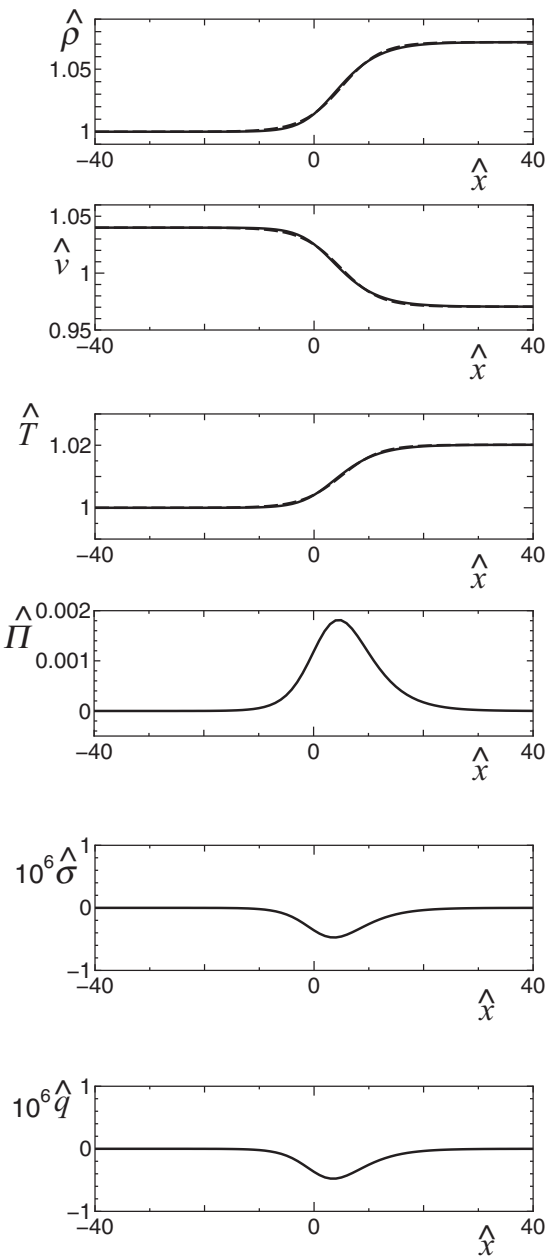

FIG. 3. Type A: Profiles of the dimensionless mass density, velocity, temperature, dynamic pressure, shear stress, and heat flux predicted by the ET theory (solid curves). Profiles of the dimensionless mass density, the dimensionless velocity, and the temperature predicted by the NSF theory (dashed curves) are also shown. $M_0 = 1.04$. The conditions for the numerical calculations are $\hat{L} = 100$ and $N = 100$.

We notice that the thickness of a shock wave is very large, even at the order of several centimeters, because of the large characteristic length estimated as $\tau_\Pi(\rho_0, T_0)c_0 = 0.60$ cm. The dimensionless dynamic pressure is also several orders of magnitude larger than the dimensionless shear stress and heat flux. These features are, of course, due to the fact that the relaxation time for the dynamic pressure τ_Π, which is proportional to the bulk viscosity ν, is much larger than the other two relaxation times τ_S and τ_q which are, respectively, proportional to the shear viscosity μ and the heat conductivity κ. Because of the large thickness and the small Mach number, i.e., small gradients of physical quantities, the shock wave is not very far from local equilibrium. Therefore the predictions from the present ET theory and the predictions from the NSF theory are similar to each other. It is this type A that Gilbarg and Paolucci [10] studied.

B. Type B: Asymmetric shock wave structure

When the Mach number increases further, the gradient of the physical quantities in the shock wave structure near the unperturbed state becomes much steeper than the gradient near the perturbed state. The shock wave structure now becomes obviously asymmetric. The NSF theory cannot describe such asymmetric profiles. A typical shock wave structure of type B is shown in Fig. 4 where $M_0 = 1.12$.

From Fig. 4, we can see that the dimensionless shear stress and the heat flux are still several orders of magnitude smaller than the dimensionless dynamic pressure in the whole range of the shock wave structure. Therefore we may conclude that the dynamic pressure plays a much more important role in the global structure of shock waves of types A and B than do the shear stress and the heat flux.

C. Type C: Shock wave structure composed of thin and thick layers

When the Mach number increases even further, the shock wave structure changes from a single-layer asymmetric structure (type B) to a structure composed of thick and thin layers (type C). Typical examples of type C are shown in Fig. 5 with $M_0 = 1.15$ and Fig. 6 with $M_0 = 1.47$. It is this type C that Bethe and Teller mainly studied. The NSF theory again cannot describe such shock wave structures with two layers.

We notice from Figs. 5 and 6 clearly that the thickness of the thin layer is finite although it is still much smaller than that of the thick layer, the thickness of which is of the order of several centimeters. Therefore we can analyze the detailed structure in the thin layer, which it is impossible to address using the Bethe-Teller theory. For example, as shown in the figures, we understand the detailed profiles of the dissipative quantities in the thin layer.

We see that the shear stress and the heat flux are negligibly small everywhere except in the thin-layer region. On the other hand, the dynamic pressure is large in both the thick and thin layers. Therefore we may say that, in the thin layer with finite thickness, all dissipative quantities together play a crucial role, while, in the thick layer, only the dynamic pressure seems to be essential.

Within the present theory, as is pointed out above, a continuous shock wave structure is obtained until $M_0 \approx 1.74$. If we want to study the shock wave structure at larger Mach numbers than 1.74 we need ET theory with more independent variables, details of which are left for future study.

D. Critical Mach numbers for the transitions of the type of shock wave structure

We have estimated numerically the critical Mach numbers for the transitions of the type of shock wave structure: The

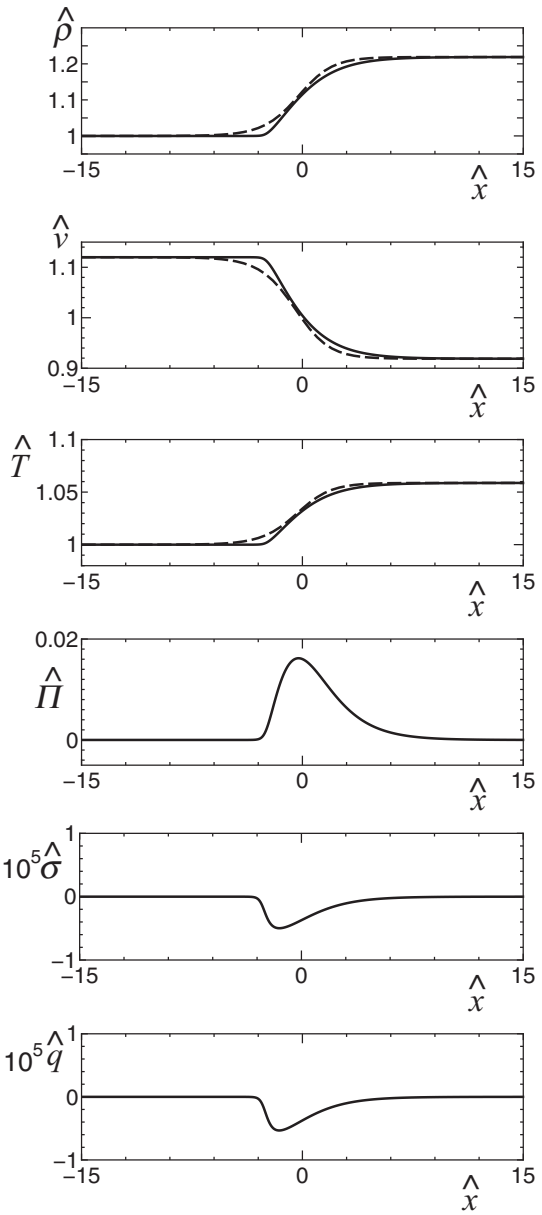

FIG. 4. Type B: Shock wave structure predicted by the ET theory (solid curves) and by the NSF theory (dashed curves). $M_0 = 1.12$. The numerical conditions are $\hat{L} = 50$, $N = 5000$ for the ET theory and $N = 100$ for the NSF theory.

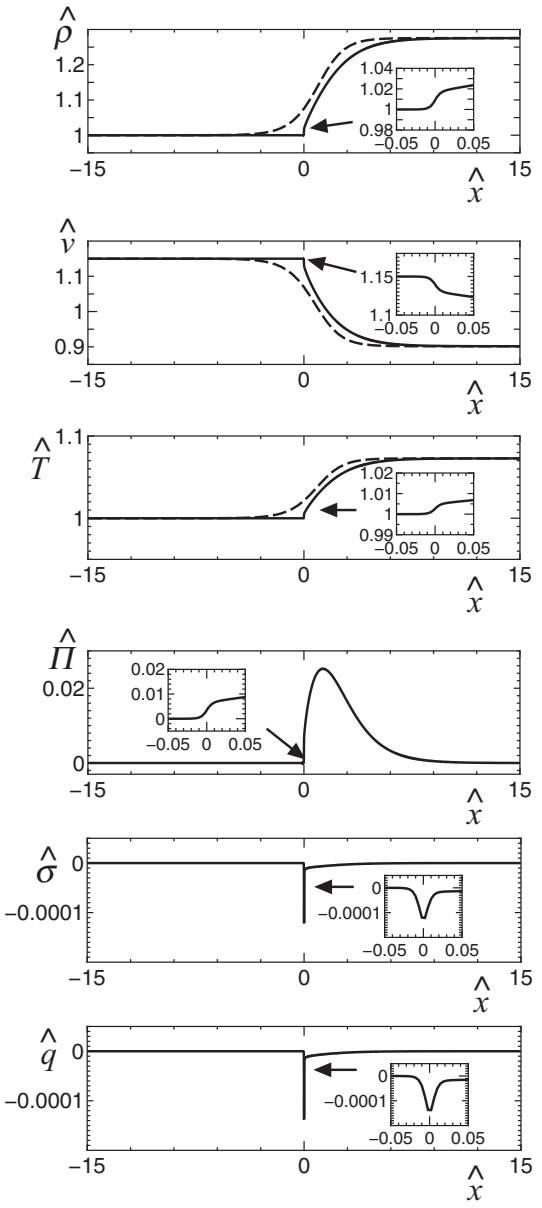

FIG. 5. Type C: Shock wave structure predicted by the ET theory (solid curves) and by the NSF theory (dashed curves). $M_0 = 1.15$. The numerical conditions are $\hat{L} = 40$, $N = 10000$ for the ET theory and $N = 100$ for the NSF theory.

asymmetric character of type B becomes evident when the Mach number is around 1.08. For the transition between type B and type C, we have the critical Mach number $M_0 \approx 1.14$. Note that these values of the Mach number are merely rough indications because the boundary between two different types cannot be clearly defined.

In the Bethe-Teller theory, from a stability analysis of the discontinuous part of the shock wave structure (nowadays known as the Lax condition [37]), the critical Mach number between type B and type C was estimated as $M_0 \approx 1.04$. This value does not agree with the value mentioned above, but is not very far from it.

E. Reexamination of the Bethe-Teller theory

Let us summarize the features of the Bethe-Teller theory in the light of the present ET theory.

(A) The Bethe-Teller theory describes the shock wave structure of type C by adopting two systems of equations under the assumption that the internal degrees of freedom of a molecule can be divided into two parts, that is, an inert part and an active part. One system is applied to analyze the thin layer and the other system is applied to the thick layer. The compatibility of the two systems of equations is, however, not self-evident. In the ET theory, on the other hand, a single system of equations can describe all types A to C without any ambiguity. There is no compatibility problem.

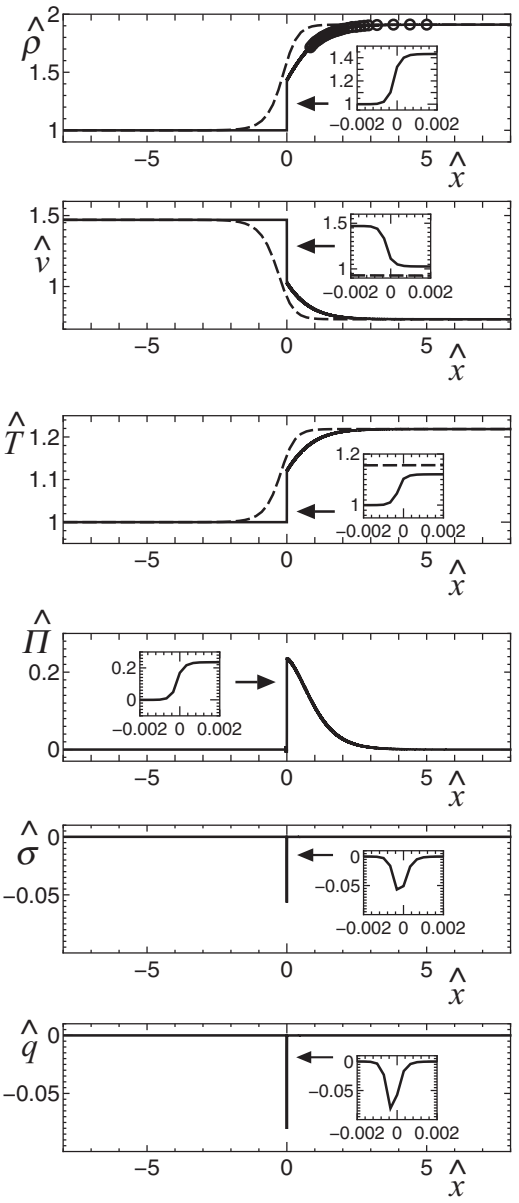

FIG. 6. Type C: Shock wave structure predicted by the ET theory (solid curves) and by the NSF theory (dashed curves). Experimental data [7] in the thick layer are also shown by circles. $M_0 = 1.47$. The numerical conditions are $\hat{L} = 20$, $N = 60000$ for the ET theory and $N = 100$ for the NSF theory.

(B) In the Bethe-Teller theory the thin layer is a jump discontinuity with zero thickness, while, in the ET theory, the thin layer has a structure with finite thickness.

(C) In the Bethe-Teller theory the thick layer is described essentially by a relaxation equation with a finite relaxation time. If necessary, the theory may be generalized so as to have several relaxation equations with different relaxation times. Usually the relaxation equation is assumed to be linear. The ET theory includes, in a natural way, the relaxation mechanism of the internal degrees of freedom [30].

(D) The critical Mach number between type B and type C can be estimated by a stability analysis. Its values as predicted by the Bethe-Teller theory and by the ET theory are not far from each other.

(E) There is a qualitative difference between the Bethe-Teller theory and the ET theory in the temperature profile. The temperature just after the discontinuous jump derived from the Bethe-Teller theory might be larger than the temperature in the perturbed state, while the temperature profile derived from the ET theory is always smaller than the perturbed temperature.

Experiments to observe the temperature profile, however, seem to be extremely difficult because a shock wave has a very steep and rapid change in space and time. There is another difficulty from a theoretical point of view. We should be careful about the definition of the temperature in nonequilibrium. See Ref. [23] for a discussion of the definition of the temperature in nonequilibrium in the ET theory.

VI. COMPARISON OF THE PRESENT RESULTS WITH EXPERIMENTAL DATA

Experiments on the shock wave structure in CO_2 gas at room temperature and atmospheric pressure indicate that shock profiles with no thin layer are obtained at least in the range $1 < M_0 < 1.04$ [8]. The present result is consistent with this.

Experimental results at $M_0 = 1.134$ and $M_0 = 1.16$ are available [5,6]. We have confirmed that our theoretical predictions shown in Fig. 5 are qualitatively the same as the shock profiles obtained in the experiments. Quantitative comparison is, however, impossible because only the interferograms are shown in the experimental papers.

Experimental data for the mass density profile [7] and the theoretical mass density profile derived from the ET theory at $M_0 = 1.47$ are shown in Fig. 6. Note that only the experimental data in the thick layer are reported in the paper, in which the authors said that accurate measurement in the region near the thin layer was impossible because the change of physical quantities is so steep. In order to study the data in more detail, Fig. 6 is presented in a different way: a single logarithmic plot of the profile of the mass density difference $\hat{\rho}_1 - \hat{\rho}$ as shown in Fig. 7. We can see that the agreement between the theoretical prediction and the experimental data is excellent. It is also remarkable that the ET theory seems to explain the deviation of the experimental data $\hat{\rho}_1 - \hat{\rho}$ from the dotted line in Fig. 7, i.e., from a purely exponential decay.

Unfortunately, experimental data for the mass density profile at $M_0 = 1.47$ only are available at present. More detailed experimental studies of the shock wave structure are expected.

VII. SUMMARY AND OUTLOOK

In this paper, we have developed a thermodynamic theory of the shock wave structure in a rarefied polyatomic gas by using ET14 theory with a hyperbolic system of 14 field equations. The ET14 theory can describe the three types of shock wave structure, types A to C, consistently. It has been shown that, in the case of CO_2 gases, the theoretical predictions are consistent with experimental data. The Bethe-Teller theory and the Gilbarg-Paolucci theory of the shock wave structure

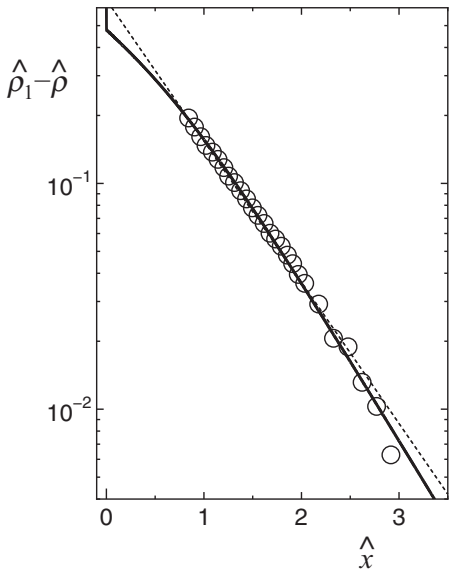

FIG. 7. Profile of the mass density difference $\hat{\rho}_1 - \hat{\rho}$ predicted by the ET theory (solid curve) and the experimental data (circles) [7]. The dotted line shows an exponential decay.

in a polyatomic gas have also been critically discussed in the light of the present theory.

We have found that the dynamic pressure Π is essentially important in the shock wave structure but the shear stress and the heat flux are not so important everywhere except inside a thin layer. Therefore it is natural to expect that, by neglecting all dissipative fluxes but the dynamic pressure, we can study the shock wave structure properly. In fact, we have shown recently that the ET theory with six independent fields (ET6) can describe the shock wave structure of types A to C reasonably well [38].

Lastly we summarize the outlook for future research as follows:

(i) The ET theory is different from the usual theories adopted in the literature of gas dynamics [1,2]. We expect that gas dynamics theory can be reformulated and developed by using the ET theory.

(ii) The shock wave structure in various kinds of gases is now being studied using ET theory. For example, shock waves in hydrogen gas appear interesting because the specific heat of the gas has a peculiar temperature dependence due to the quantum effect. The isotope effect on the shock wave structure is also interesting. We are also interested in the shock wave structure in nitrogen gas. Because the rotational modes are fully excited but the vibrational modes are little excited at room temperature, a thin shock wave structure is observed [39]. The ET theory is expected to be useful for analyzing such thin shock wave structures. The details of the studies will soon be reported.

(iii) The shock wave structure in a dense gas is the next subject to be studied by ET theory, using the virial expansion form of the equations of state.

(iv) Analyses of contact waves and rarefaction waves, in addition to shock waves, are also among future studies. We are planning to solve the Riemann problem in order to confirm whether the conjecture proposed by Brini and Ruggeri [40,41] is valid or not in ET systems.

ACKNOWLEDGMENTS

This work was partially supported by Japan Society of Promotion of Science (JSPS) Grants No. 24760055 (S.T.) and No. 25390150 (M.S.) and by the National Group of Mathematical Physics GNFM-INdAM (T.R.).

APPENDIX: NAVIER-STOKES FOURIER THEORY

The NSF system of equations in the present analysis is obtained as the first approximation of the ET14 system (6) by using the Maxwellian iteration [23,42]:

$$\begin{aligned}
&\frac{\partial \rho}{\partial t} + \frac{\partial}{\partial x}(\rho v) = 0,\\
&\frac{\partial \rho v}{\partial t} + \frac{\partial}{\partial x}(p + \Pi - \sigma + \rho v^2) = 0,\\
&\frac{\partial}{\partial t}(2\rho\varepsilon + \rho v^2) + \frac{\partial}{\partial x}\{2\rho\varepsilon v + 2(p + \Pi - \sigma)v\\
&\quad + \rho v^3 + 2q\} = 0,\\
&\Pi = -\left(\frac{2}{3} - \frac{1}{\hat{c}_v}\right) p\tau_\Pi \frac{\partial v}{\partial x},\\
&\sigma = \frac{4}{3} p\tau_S \frac{\partial v}{\partial x}, \quad q = -(1 + \hat{c}_v)\frac{k_B}{m} p\tau_q \frac{\partial T}{\partial x}.
\end{aligned} \tag{A1}$$

From eqs. $(A1)_{4-6}$, we obtain the relationship between relaxation times and the phenomenological coefficients (7). Note that the system (A1) is of parabolic type although the original ET system (6) is hyperbolic.

The dimensionless forms of the conservation laws are the same as $(11)_{1-3}$, while the dimensionless constitutive relations are expressed by

$$\begin{aligned}
&\hat{\Pi} = -\left(\frac{2}{3} - \frac{1}{\hat{c}_v(T)}\right)\frac{M_0\hat{T}}{\hat{v}}\hat{\tau}_\Pi \frac{d\hat{v}}{d\hat{x}},\\
&\hat{\sigma} = \frac{4}{3}\frac{M_0\hat{T}}{\hat{v}}\hat{\tau}_S \frac{d\hat{v}}{d\hat{x}},\\
&\hat{q} = -[1 + \hat{c}_v(T)]\frac{1}{\gamma_0}\frac{M_0\hat{T}}{\hat{v}}\hat{\tau}_q \frac{d\hat{T}}{d\hat{x}}.
\end{aligned} \tag{A2}$$

The theoretical predictions of the NSF theory are depicted in Figs. 3 to 6.

[1] W. G. Vincenti and C. H. Kruger, Jr., *Introduction to Physical Gas Dynamics* (John Wiley and Sons, New York, 1965).

[2] Ya. B. Zel'dovich and Yu. P. Raizer, *Physics of Shock Waves and High-Temperature Hydrodynamic Phenomena* (Dover Publications, Mineola, NY, 2002).

[3] E. F. Smiley, E. H. Winkler, and Z. I. Slawsky, J. Chem. Phys. **20**, 923 (1952).

[4] E. F. Smiley and E. H. Winkler, J. Chem. Phys. **22**, 2018 (1954).

[5] W. C. Griffith and W. Bleakney, Am. J. Phys. **22**, 597 (1954).

[6] W. Griffith, D. Brickl, and V. Blackman, Phys. Rev. **102**, 1209 (1956).

[7] N. H. Johannesen, H. K. Zienkiewicz, P. A. Blythe, and J. H. Gerrard, J. Fluid Mech. **13**, 213 (1962).

[8] W. C. Griffith and A. Kenny, J. Fluid Mech. **3**, 286 (1957).

[9] H. A. Bethe and E. Teller, *Deviations from Thermal Equilibrium in Shock Waves* (1941; reprinted Engineering Research Institute, University of Michigan), https://www.fas.org/sgp/othergov/doe/lanl/lib-www/la-pubs/00367149.pdf.

[10] D. Gilbarg and D. Paolucci, J. Rational Mech. Anal. **2**, 617 (1953).

[11] S. R. de Groot and P. Mazur, *Non-Equilibrium Thermodynamics* (North-Holland, Amsterdam, 1963).

[12] S. Chapman and T. G. Cowling, *The Mathematical Theory of Non-Uniform Gases* (Cambridge University Press, Cambridge, 1991).

[13] H. Grad, Pure Appl. Math. **2**, 331 (1949).

[14] I. Müller and T. Ruggeri, *Rational Extended Thermodynamics*, 2nd ed. (Springer, New York, 1998).

[15] I. Müller and T. Ruggeri, *Extended Thermodynamics*, 1st ed. (Springer, New York, 1993).

[16] W. Dreyer, J. Phys. A **20**, 6505 (1987).

[17] H. Struchtrup, *Macroscopic Transport Equations for Rarefied Gas Flow, Approximation Methods in Kinetic Theory* (Springer, Berlin, 2005).

[18] G. A. Bird, *Molecular Gas Dynamics and the Direct Simulation of Gas Flows* (Oxford University Press, Oxford, 1994).

[19] V. M. Zhdanov, Sov. Phys. JETP **26**, 1187 (1968).

[20] F. J. MacCormack, Phys. Fluids **11**, 2533 (1968).

[21] F. J. MacCormack, Phys. Fluids **13**, 1446 (1970).

[22] F. Mallinger, INRIA Research Report No. RR-3581, 1998 (unpublished).

[23] T. Arima, S. Taniguchi, T. Ruggeri, and M. Sugiyama, Continuum Mech. Thermodyn. **24**, 271 (2012).

[24] T. Arima, M. Sugiyama, Atti Accad. Peloritana Pericolanti **91**, Suppl. No. 1, A1 (2013).

[25] M. Pavić, T. Ruggeri, and S. Simić, Physica A **392**, 1302 (2013).

[26] T. Ruggeri, Continuum Mech. Thermodyn. **1**, 3 (1989).

[27] C. Borgnakke and P. S. Larsen, J. Comput. Phys. **18**, 405 (1975).

[28] J.-F. Bourgat, L. Desvillettes, P. Le Tallec, B. Perthame, Eur. J. Mech. B/Fluids **13**, 237 (1994).

[29] T. Arima, S. Taniguchi, T. Ruggeri, and M. Sugiyama, Continuum Mech. Thermodyn. **25**, 727 (2013).

[30] T. Arima, S. Taniguchi, T. Ruggeri, and M. Sugiyama, Phys. Lett. A **376**, 2799 (2012).

[31] J. Meixner, Ann. Phys. (N.Y.) **435**, 470 (1943).

[32] J. Meixner, Acoustica **2**, 101 (1952).

[33] G. Boillat and T. Ruggeri, Continuum Mech. Thermodyn. **10**, 285 (1998).

[34] *JSME Data Book: Thermophysical Properties of Fluids* (Japan Society of Mechanical Engineers, Tokyo, 1983).

[35] *CRC Handbook of Chemistry and Physics,* 91st ed., edited by W. M. Haynes and D. R. Lide (CRC Press, Boca Raton, FL, 2010).

[36] W. Weiss, Phys. Rev. E **52**, R5760 (1995).

[37] P. Lax, Commun. Pure Appl. Math. **10**, 537 (1957).

[38] S. Taniguchi, T. Arima, T. Ruggeri, and M. Sugiyama, Phys. Fluids **26**, 016103 (2014).

[39] H. Alsmeyer, J. Fluid Mech. **74**, 497 (1976).

[40] F. Brini and T. Ruggeri, Suppl. Rend. Circ. Mat. Palermo II **78**, 31 (2006).

[41] A. Mentrelli and T. Ruggeri, Suppl. Rend. Circ. Mat. Palermo II **78**, 201 (2006).

[42] E. Ikenberry and C. Truesdell, J. Rational Mech. Anal. **5**, 1 (1956).